Micromechanics-Based Optimization of Pigmentable Strain-Hardening Cementitious Composites

En-Hua Yang, A.M.ASCE[1]; Estela O. Garcez[2]; and Victor C. Li, F.ASCE[3]

Abstract: Architectural and decorative concrete (ADC) has become an enormously popular product for both building interiors and exteriors, combining an aesthetic finish with structural capabilities. Cracking and chipping of ADC product during handling and transportation, however, is of great concern due to the brittleness of ADC materials. This paper looks at the development of a white strain-hardening cementitious composite (SHCC) as an alternative ADC material to address the above-mentioned challenges. It was found that the replacement of ordinary portland cement and fly ash with white cement altered SHCC microstructure which is unfavorab to the tensile strain-hardening behavior. A micromechanical model was engaged for composite optimization through ingredients selection and component tailoring to reengineer white SHCCs. **DOI: 10.1061/(ASCE)MT.1943-5533.0000914.**

Author keywords: Architectural and decorative concrete; White cement; Engineered cementitious composites (ECC).

Introduction

Recent development in pigmenting technology (U.S. Patent No. 5,795,513) has made it possible to create cement-based manufactured stone with a pattern and texture similar to that of natural rocks. This type of concrete is generally known as architectural and decorative concrete (ADC) (Li and Tian 2010). One fundamental requirement for ADC is that the material should be pigmentable. In general, that means a white color base material is required before pigmenting. To achieve this goal, white cement is generally used to replace the grayish ordinary portland cement in preparing ADC. White clinker can be produced by carefully selecting the raw materials, i.e., iron-free clay and white limestone, in the clinkering process. The content of ferrous composites and other heavy-metal composites in the raw materials must not exceed 0.15% to give the distinctive white color (Mindess et al. 2002). ADC made with white cement enables the resulting concrete to be pigmentable for a broad spectrum of colors (Cassar et al. 2003).

Materials used for the ADC are often high-strength mortar or high-strength concrete. The brittleness of cement-based material, however, contributes to the chipping and fragmentation of ADC product during handling and transportation and is of great concern. Strain-hardening cementitious composites (SHCC) is a new class of concrete material featuring tensile strain-hardening behavior after first cracking. Fig. 1 shows the typical tensile stress-strain curve of engineered cementitious composites (ECC) made of gray ordinary portland cement (OPC) and fly ash; a unique SHCC exhibits extreme tensile ductility several hundred times that of normal concrete with the inclusion of a relatively low fiber dosage of 2 vol.% or less. ECC can be a potential material solution for preventing chipping and fragmentation, eliminating reinforcement, and reducing the thickness of ADC products.

ECC used Type I portland cement and other mineral admixtures, such as fly ash, as binders (Yang et al 2007). The resulting ECC was grayish and was not ideal for pigmentation. The objective of this paper was to develop a white ECC as an alternative ADC material. In the following sections, white ECC design framework was introduced first, followed by the introduction of micromechanics-based strain-hardening model. This analytical model was used to guide ingredient selection and component tailoring to develop a pigmentable version of ECC.

White ECC Design Framework

The design framework of white ECC was based on the concept of scale linking as shown in Fig. 2, in which macroscopic composite tensile strain-hardening behavior was governed by the mesoscopic fiber bridge properties. The fiber-bridging properties were further determined by the microscopic characteristics of fiber, matrix, and interface. Analytical models described in the next section link constituent parameters in microscale to composite tensile strain-hardening behavior in macroscale. The model-based linking provided a tool for ingredient selection and component tailoring, which allows systematic composite optimization for maximum tensile ductility with the minimum amount of fibers. This conceptual framework represented a holistic approach in white ECC design accounting for the interaction between the fiber, matrix, and interface.

Micromechanics-Based Strain-Hardening Analytical Model

The fundamental requirement for composite tensile strain-hardening was that steady-state crack propagation prevailed under tension, which required the crack tip toughness J_{tip} to be less than the complementary energy J_b' calculated from the bridging stress σ versus crack opening δ curve, as illustrated in Fig. 3 (Marshall and Cox 1988; Li and Leung 1992)

[1]Assistant Professor, Nanyang Technological Univ., Singapore 639798 (corresponding author). E-mail: ehyang@ntu.edu.sg

[2]Professor, Federal Univ. of Rio Grande do Sul, 110, Farropilhas, Porto Alegre - Rio Grande do Sul 90040-060, Brazil. E-mail: estelagarcez@gmail.com

[3]Professor, Univ. of Michigan, Ann Arbor, MI 48109. E-mail: vcli@umich.edu

Note. This manuscript was submitted on April 10, 2013; approved on July 31, 2013; published online on August 3, 2013. Discussion period open until August 20, 2014; separate discussions must be submitted for individual papers. This paper is part of the ***Journal of Materials in Civil Engineering***, © ASCE, ISSN 0899-1561/04014017(6)/$25.00.

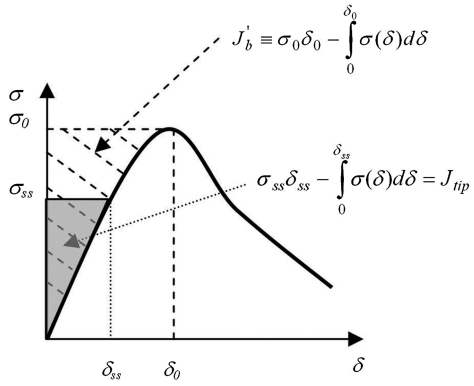

Fig. 3. Typical $\sigma(\delta)$ curve for tensile strain-hardening composite; hatched area represents complimentary energy J_b'; shaded area represents crack tip toughness J_{tip}

Fig. 1. A typical uniaxial tensile stress–strain curve of Gray OPC ECC (concrete strain 10 times expanded is shown as control)

$$J_{\text{tip}} \leq \sigma_0\delta_0 - \int_0^{\delta_0}\sigma(\delta)d\delta \equiv J_b' \tag{1}$$

$$J_{\text{tip}} = \frac{K_m^2}{E_m} \tag{2}$$

where σ_0 = the maximum bridging stress corresponding to the opening δ_0; K_m = the matrix fracture toughness; and E_m = the matrix Young's modulus. Eq. (1) employed the concept of energy balance during flat crack extension between external work, crack tip energy absorption through matrix breakdown (matrix toughness), and crack flank energy absorption through fiber/matrix interface debonding and sliding. This energy-based criterion determined that the crack shall propagate in a steady-state flat mode or in a Griffith mode (Yang and Li 2007).

The stress–crack opening relationship $\sigma(\delta)$, which can be viewed as the constitutive law of fiber bridging behavior, was derived by using analytic tools of fracture mechanics, micromechanics, and probabilistics. In particular, the energetics of tunnel crack propagation along fiber/matrix was used to quantify the debonding process and the bridging force of a fiber with given embedment length (Lin et al. 1999). Probabilistics was introduced to describe the randomness of fiber location and orientation with respect to a crack plane. The random orientation of fiber also necessitated the accounting of the mechanics of interaction between an inclined fiber and the matrix crack. As a result, the $\sigma(\delta)$ curve was expressible as a function of micromechanics parameters, including interface chemical bond G_d, interface frictional bond τ_0, and slip-hardening coefficient β accounting for the slip-hardening behavior during fiber pullout. In addition, snubbing coefficient f and strength reduction factor f' were introduced to account for the interaction between fiber and matrix as well as the reduction of fiber strength when pulled at an inclined angle. Besides interfacial properties, the $\sigma(\delta)$ curve was also governed by the matrix Young's modulus E_m, fiber content V_f, and fiber diameter d_f, length L_f, and Young's modulus E_f.

Another condition for the pseudo strain-hardening was that the matrix tensile cracking strength σ_c must not exceed the maximum fiber bridging strength σ_0

$$\sigma_c < \sigma_0 \tag{3}$$

where σ_c was determined by the matrix fracture toughness K_m and preexisting internal flaw size a_0.

While the energy criterion [Eq. (1)] governed the crack propagation mode, the strength-based criterion represented by Eq. (3) controlled the initiation of cracks. Satisfaction of both Eqs. (1) and (3) was necessary to achieve tensile strain-hardening behavior; otherwise, normal tension-softening behavior results. In addition, due to the random nature of preexisting flaw size and fiber distribution in cement composites, a margin between J_b' and J_{tip} as well as σ_c and σ_0 was necessary to ensure saturated multiple cracking and robust tensile strain-hardening behavior (Kanda 1998). In the design of white ECC, $J_b'/J_{\text{tip}} > 2$ and $\sigma_0/\sigma_c > 1.15$ were used (Yang and Li 2010). Details of these micromechanical analyses can be found in previous works (Lin et al. 1999; Li 1992).

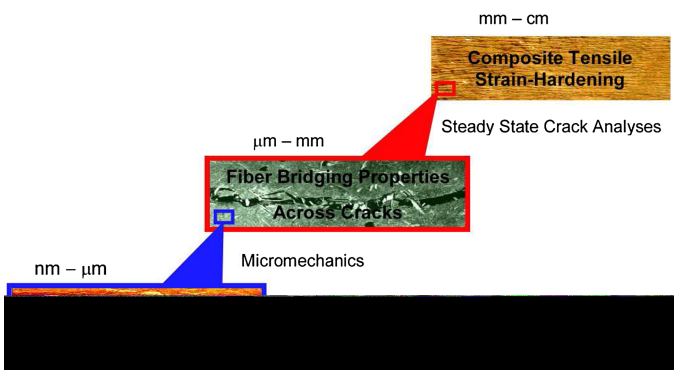

Fig. 2. White ECC design framework—scale linking

Experimental Program

Materials and Mix Design

Mix design of white ECCs was summarized in Table 1. OPC and fly ash were replaced with white cement. White portland cement Type I was obtained from Lehigh white cement. White microsilica sand with a maximum grain size of 250 μm and an average size of 110 μm was adopted in the mixture. A polycarboxylate-based high-range water reducer produced by W.R. Grace was used in this study.

Table 1. Mix Design of White ECCs by Mass

Material	Cement	Sand	Water	Superplasticizer	PVA fiber (by volume)
White ECC v1	1	1	0.34	0.004	0.02
White ECC v2	1	0.5	0.31	0.004	0.025
White ECC v3	1	0.5	0.31	0.003	0.02
White ECC v4	1	0.5	0.31	0.003	0.02

Table 2. PVA Fiber Length and Surface Oiling Content Used in White ECCs

Material	Fiber length (mm)	Fiber surface oiling content (wt.%)
White ECC v1	8	1.2
White ECC v2	8	1.2
White ECC v3	12	1.2
White ECC v4	12	0.5

Micro polyvinyl alcohol (PVA) fiber REC-15 was produced by Kuraray Co., Japan. The diameter of the micro PVA fiber was 39 μm on average, and the nominal tensile strength and the density of the fiber were 1,600 MPa and 1,300 kg/m^3, respectively. Fibers with various length and surface oiling content were used as a means to control fiber bridging properties, which result in distinct tensile strain-hardening behavior of white ECCs. The selection of fiber length and surface oiling content was guided by micromechanical models and was discussed in Section 5. Table 2 summarizes the specifications of PVA fibers used in the four versions of white ECCs.

Mixing and Curing

A planetary mixer with 20 L capacity was used in preparing all white ECC mixtures. Solid ingredients, including white cement and white microsilica sand, were first mixed for a couple of minutes. Water and high-range water-reducing admixture were then added into the dry mixture and mixed for another 3 min. The liquefied fresh mortar matrix should reach a consistent and uniform state before adding fibers. After examining the mortar matrix and making sure there is no clump in the bottom of the mixer, PVA fibers were slowly added into the mortar matrix and mixed until all fibers were evenly distributed. The mixture was then cast into molds. Specimens were demolded after 24 h. After demolding, specimens were first cured in sealed bags at room temperature (23 $\pm$ 2°C) for three days followed by curing in air at room temperature before testing at the age of 28 days. The relative humidity of the laboratory air was 45% $\pm$ 5%.

Specimens and Tests

The 28 days compression test was carried out on cylinders measuring 75 mm in diameter and 150 mm in length following ASTM C39 standard. The cylinders' ends were capped with a sulfur compound to ensure a flat and parallel surface and a better contact with the loading device. The tensile stress-strain behavior at the age of 28 days was determined from direct uniaxial tensile tests in coupon specimens measuring 152 mm by 76 mm by 13 mm following procedures described in Yang et al. (2007). A servo hydraulic testing system was used in displacement control mode to conduct the tensile test. The loading rate used was 0.0025 mm/s to simulate a quasi-static loading condition.

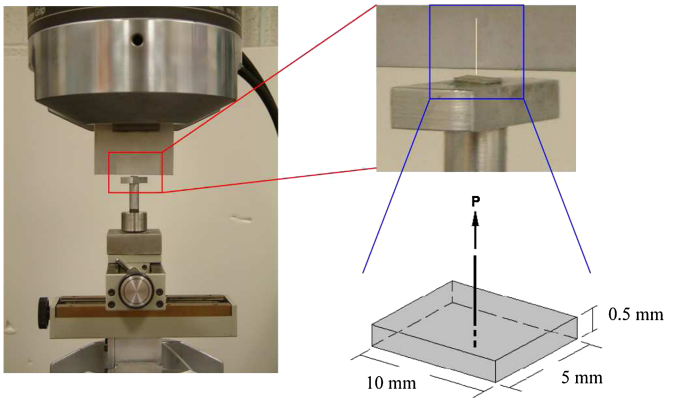

Fig. 4. Test setup of single fiber pullout test

Single-fiber pullout tests as shown in Fig. 4 were performed to quantify fiber/matrix interfacial properties, including chemical bond strength G_d, frictional bond strength τ_0, and slip-hardening coefficient β. Specimen preparation, test configuration, data processing, and calculation of interfacial parameters can be found in Redon et al. (2001). The measured interfacial parameters were then used as inputs for calculation of fiber-bridging law $\sigma(\delta)$ and to evaluate the tensile strain-hardening performance of white ECCs. The results were then used to guide ingredient selection and component tailoring for microstructure optimization of white ECCs.

Results and Discussion

First Attempt to Produce White ECC: Version 1

Table 3 summarized mechanical properties of the four white ECCs at the age of 28 days. Fig. 5 showed the uniaxial tensile stress–strain curves of white ECC v1. As can be seen, white ECC v1 exhibited moderate tensile strain-hardening behavior with an average tensile strain capacity of 1.2% and an average tensile strength of 5.9 MPa. Compared to gray OPC ECC (Fig. 1), however, white ECC v1 showed a significant reduction (60%) in tensile ductility. Microscopic observation of the fracture surface of white ECC v1 revealed that most of the PVA fibers were pulled out instead of rupture as shown in Fig. 6. This suggested the interfacial bond of white ECC is lower than that of gray OPC ECC as a result of the replacement of ordinary portland cement and fly ash with white cement.

Fiber/Matrix Interface Properties of Gray and White ECC

Table 4 summarized the interfacial properties of gray OPC ECC and white ECC v1 obtained from the single fiber pullout tests. As can be seen, the interface chemical bond of white ECC v1 was comparable to that of gray OPC ECC. The interface frictional bond

Table 3. Mechanical Properties of White ECCs at the Age of 28 Days

Mechanical properties	White ECC			
	v1	v2	v3	v4
ε_{ult} (%)	1.3 $\pm$ 0.1	0.6 $\pm$ 0.1	1.7 $\pm$ 0.8	2.7 $\pm$ 0.4
σ_{ult} (MPa)	5.7 $\pm$ 0.3	6.7 $\pm$ 0.2	6.3 $\pm$ 0.5	6.7 $\pm$ 0.1
f_c' (MPa)	60	55	59	65

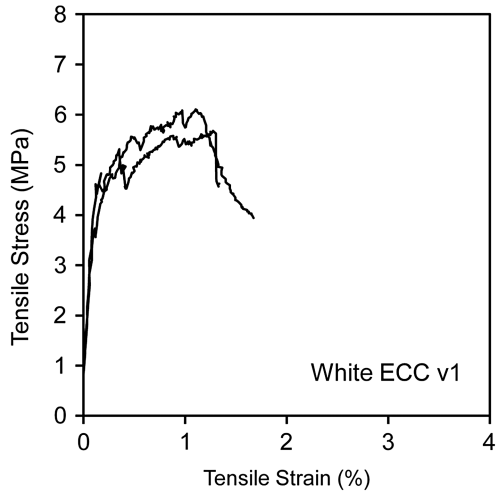

Fig. 5. Uniaxial tensile stress–strain curves of white ECC v1

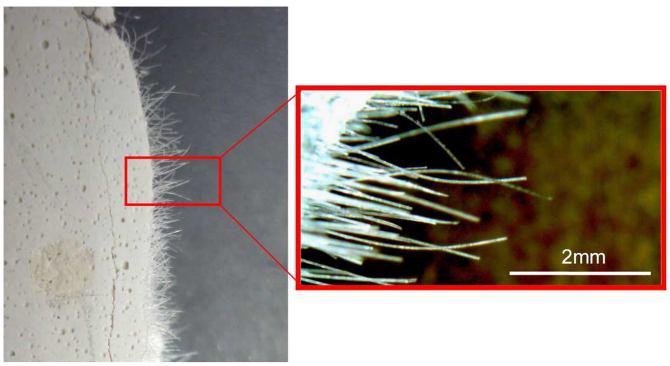

Fig. 6. Microscopic observation of fracture surface of white ECC v1

Table 4. Fiber/Matrix Interfacial Properties of ECCs

Material	G_d (J/m^2)	τ_0 (MPa)	β
Gray OPC ECC	1.08 ± 0.69	2.27 ± 0.89	0.58 ± 0.22
White ECC v1	1.06 ± 0.19	1.18 ± 0.26	0.56 ± 0.22

of white ECC v1, however, was drastically reduced, only about half that of gray OPC ECC. This can be attributed to the exclusion of fly ash in white ECC, which prohibited the pozzolanic reaction and resulted in a loose interface transition zone (ITZ) and a lower interface frictional bond between the fiber/matrix interface (Yang et al. 2007).

Micromechanics-Based Component Tailoring

To evaluate the impact of lower frictional bond on the tensile strain-hardening behavior of white ECC v1, micromechanics-based analytical models described in Section 3 were used to calculate the critical fiber volume of achieving tensile strain-hardening as a function of interface frictional bond. Fig. 7 showed the calculation results. The two curves in Fig. 7(a) relating V_{crit}^f to τ_0 were calculated by specifying all other measured micromechanical parameters in Eqs. (1) and (3), respectively.

As can be seen from Fig. 7(a), V_{crit}^f calculated from the strength criterion En. (3) (solid line) approached a constant at high frictional bond and sharply increased at low friction area ($\tau_0 < 0.7$ MPa). The bridging strength was known to be governed by fiber strength, fiber volume, and interfacial properties, e.g., τ_0 and G_d. At higher interfacial friction, however, fiber rupture dominated over fiber pullout so the bridging strength became insensitive to τ_0. Because fiber strength was given, fiber volume approaches to a steady value to satisfy the strength criterion. At low friction, however, fiber pullout prevailed over fiber rupture, and bridging strength was now insensitive to the fiber strength and governed by fiber volume and τ_0. A high amount of fiber was therefore required to obtain adequate bridging strength.

On the other hand, a concave V_{crit}^f curve was obtained based on the energy criterion En. (1) (dashed line). The bridging strength decreased with the reduction of τ_0, resulting in the low J_b', shaded area in Fig. 3, at low τ_0 region. At high τ_0, the stiffness of the fiber bridging springs [i.e., the initial slope of the $\sigma(\delta)$] kept rising, resulting in a decrease in J_b' as well. High fiber fraction was therefore required at both high and low τ_0 to satisfy the energy criterion. An optimum point, i.e., a balanced interfacial friction (τ_0 around 1.1 MPa), which met the specified J_b' at minimum fiber fraction, existed in the energy curve.

Strain-hardening behavior relied on the satisfaction of both the strength and the energy criteria. Therefore, the minimum fiber amount to achieve saturated multiple cracking was the combination of the two curves, whichever has a higher V_{crit}^f as depicted in Fig. 7(b). Materials in the area above the curve shall exhibit strong

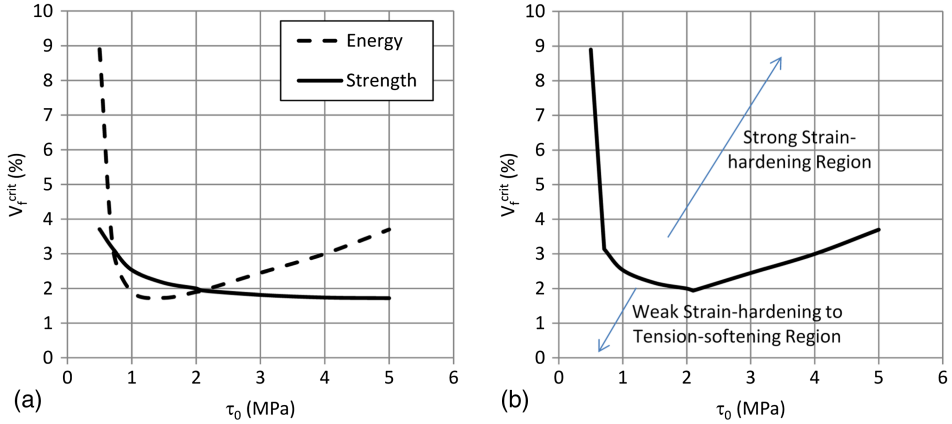

Fig. 7. V_f^{crit} as a function of τ_0 determined by (a) the energy and the strength criterion, respectively; (b) the combined curve

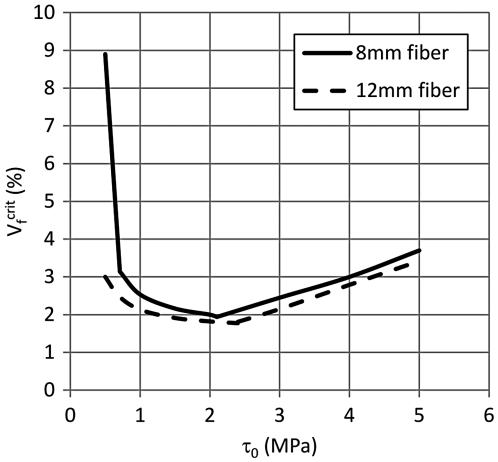

Fig. 8. Effect of fiber length on the V_f^{crit}

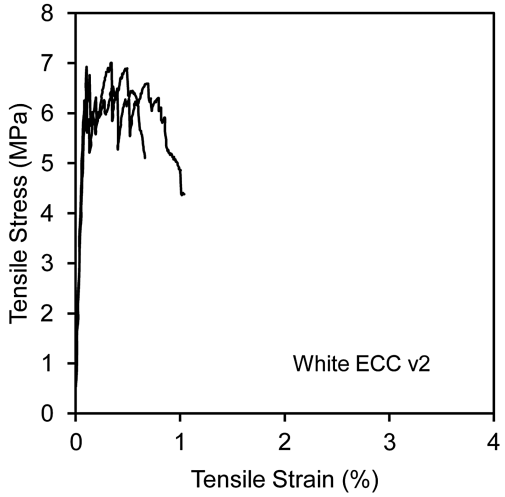

Fig. 9. Uniaxial tensile stress–strain curves of white ECC v2

and robust tensile strain-hardening behavior because a margin of $J_b'/J_{\text{tip}} > 2$ and $\sigma_0/\sigma_c > 1.15$ were used in the calculation. Materials in the area below the curve, on the other hand, shall exhibit weak tensile strain-hardening or tension-softening behavior. As can be seen, the most economical design point (i.e., minimum V_f^{crit}) for tensile strain-hardening was at 1.94 vol.% of fiber content with 2.1 MPa of interface frictional bond strength, which was the design basis for gray OPC ECC ($\tau_0 = 2.27$ MPa, 2 vol.% fiber).

In the case of white ECC v1, the interface frictional bond reduced to 1.18 MPa. The required critical fiber volume for robust tensile strain-hardening behavior was predicted to be 2.5 vol.%. Based on the guidance of this exercise, it was possible to improve the strain-hardening behavior of white ECC by increasing the fiber volume to 2.5 vol.% or by increasing the frictional bond of white ECC to 2 MPa while maintaining the fiber volume to 2 vol.%. Increase of the interface frictional bond can be achieved through the adoption of a lower oil coating on the surface of PVA fibers (Li et al. 2002). Fig. 8 showed the effect of fiber length on the V_{crit}^f curve. As can be seen, the V_{crit}^f curve of the 12 mm PVA fiber dropped significantly at low τ_0. It suggested that adopting the 12 mm PVA fiber could also improve the strain-hardening behavior of white ECC.

White ECC Re-Engineering: Versions 2–4

Based on the insights gained from the analytical model, white ECC v2–v4 were developed as shown in Table 1. As can be seen in Table 2, white ECC v2 adopted the strategy of higher fiber dosage (2.5 vol.%), while white ECC v3 incorporated the strategy of longer fibers (12 mm). White ECC v4 adopted a combined strategy of longer fibers and increased interface frictional bond strength through lowering the fiber surface oil coating (0.5 wt.%).

Fig. 9 illustrated the uniaxial tensile stress–strain curves of white ECC v2 specimens. As can be seen, Version 2 exhibited weak tensile strain-hardening behavior with an average tensile strain capacity of 0.6% and an average tensile strength of 6.7 MPa. Despite adopting high volumes of fiber, which theoretically should give a higher bridging capacity, the mechanical properties of Version 2 did not surpass those of the first version. This may be attributed to the difficulty of processing when a higher dosage of microfibers was used, resulting in poor fiber dispersion as observed during mixing and weak fiber bridging. Fiber clumps were observed during mixing. Those fiber clumps could be treated as defects resulting in lower compressive strength of white ECC v2.

As shown in Fig. 10, white ECC v3 incorporating longer fibers exhibited improved tensile strain strain-hardening behavior with a tensile ductility of 2.0% and an average tensile strength of 6.4 MPa. Compared to white ECC v1, the tensile strength and the tensile strain capacity of white ECC v3 were improved by 66% and 8%, respectively. This can be attributed to the enhancement of fiber bridging capacity in Version 3 as a result of the incorporation of longer fibers. As predicted from the analytical model (Fig. 8), engaging longer fiber was especially beneficial for SHCC with low interface frictional bond to achieve tensile strain-hardening behavior. At low interface frictional bond, increased fiber length provided more efficient load transfer from one side of the crack surface to the other side of the crack surface through fiber/matrix interface.

The combination of longer fiber and increased frictional bond was used in the production of white ECC v4. Fig. 11 showed the tensile stress–strain curves of the white ECC v4 specimens. As predicted by the analytical model, Version 4 exhibited a much-improved tensile strain-hardening behavior with an average tensile strain capacity of 2.7% and an average tensile strength of 6.7 MPa. Compared to the first version, the tensile strain capacity and the tensile strength of Version 4 are enhanced by 125% and 14%, respectively.

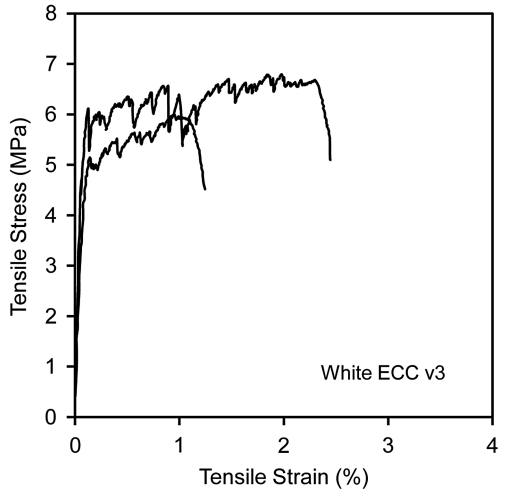

Fig. 10. Uniaxial tensile stress–strain curves of white ECC v3

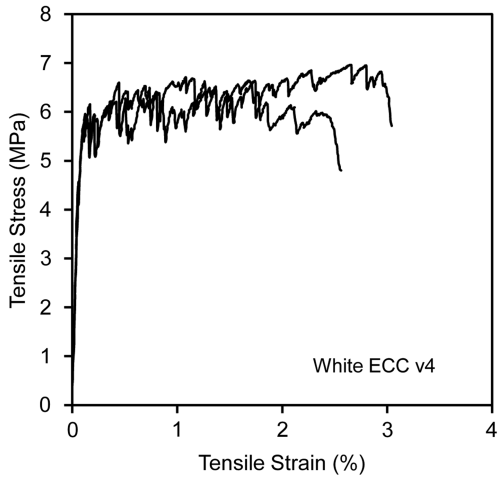

Fig. 11. Uniaxial tensile stress–strain curves of white ECC v4

Conclusions

This paper was on the development of a white engineered cementitous composite (ECC) as an alternative architectural and decorative concrete (ADC) material. White ECC allows color dyeing but imposed constraints on material ingredients that results in changes in micromechanical properties different from normal gray ECC. Specifically, white cement must be used while fly ash cannot be employed in the mix as in typical ECC formulation. This change in the matrix ingredient alters a number of micromechanical parameters, such as fiber/matrix interface properties that have strong bearing on the composite tensile properties.

It was found that the replacement of ordinary portland cement and fly ash with white cement reduced the interface fractional bond drastically, which is unfavorable to the tensile strain-hardening behavior. This was likely due to the exclusion of fly ash in white ECC which prohibits the pozzolanic reaction and resulted in a loose interface transition zone (ITZ) between the fiber/matrix interface.

Micromechanics-based composite optimization were engaged for fiber length selection and fiber surface oiling content tailoring to reengineer white ECCs with desired tensile ductility. A 125% enhancement in the tensile strain capacity (2.7%) and a 14% improvement in the tensile strength (6.7 MPa) were observed in white ECC v4 when compared with white ECC v1.

It was concluded that white cement can be successfully utilized in the production of white ECC with desired tensile properties as long as the governing mechanism was understood. Insights gained from the micromechanical models served as a guide for component tailoring and ingredient selection to achieve the desired material properties. As illustrated in this paper, the decision to increase fiber length and lower the surface oiling coating to enhance the fiber bridging capacity (and therefore the tensile ductility) in white ECC was guided by the micromechanics principles.

Acknowledgments

Support of this research by Metamorphix Global Inc. was gratefully acknowledged.

References

Cassar, L., Pepe, C., Tognon, G., Guerrini, G. L., and Amadelli, R. (2003). "White cement for architectural concrete, possessing photocatalytic properties." *11th Int. Congress on the Chemistry of Cement*, Durban, South Africa.

Kanda, T. (1998). "Design of engineered cementitious composites for ductile seismic resistant elements." Ph.D. thesis, Univ. of Michigan, Ann Arbor, MI.

Li, V. C. (1992). "Post-crack scaling relations for fiber-reinforced cementitious composites." *J. Mater. Civ. Eng.*, 10.1061/(ASCE)0899-1561(1992)4:1(41), 41–57.

Li, V. C., and Leung, C. K. Y. (1992). "Theory of steady state and multiple cracking of random discontinuous fiber reinforced brittle matrix composites." *J. Eng. Mech.*, 10.1061/(ASCE)0733-9399(1992)118:11(2246), 2246–2264.

Li, V. C., Wu, C., Wang, S., Ogawa, A., and Saito, T. (2002). "Interface tailoring for strain-hardening PVA-ECC." *ACI Mater. J.*, 99(5), 463–472.

Li, Y., and Tian, B. (2010). "Discussion on application of decorative concrete in modern architecture." *2010 Int. Conf. on Mechanic Automation and Control Engineering*, Institute of Electrical and Electronics Engineers (IEEE), Wuhan, China.

Lin, Z., Kanda, T., and Li, V. C. (1999). "On interface property characterization and performance of fiber-reinforced cementitious composites." *J. Concr. Sci. Eng.*, 1, 173–184.

Marshall, D. B., and Cox, B. N. (1988). "A J-Integral method for calculating steady-state matrix cracking stresses in composites." *Mech. Mater.*, 7(2), 127–133.

Mindess, S., Young, J. F., and Darwin, D. (2002). *Concrete*, 2nd Ed., Prentice Hall, Pearson Education, Upper Saddle River, NJ.

Redon, C., Li, V. C., Wu, C., Hoshiro, H., Saito, T., and Ogawa, A. (2001). "Measuring and modifying interface properties of PVA fibers in ECC matrix." *J. Mater. Civ. Eng.*, 10.1061/(ASCE)0899-1561(2001)13:6(399), 399–406.

Yang, E. H., and Li, V. C. (2007). "Numerical study on steady-state cracking of composites." *Compos. Sci. Tech.*, 67(2), 151–156.

Yang, E. H., and Li, V. C. (2010). "Strain-hardening fiber cement optimization and component tailoring by means of a micromechanical model." *Constr. Build. Mater.*, 24(2), 130–139.

Yang, E. H., Yang, Y. Z., and Li, V. C. (2007). "Use of high volumes of fly ash to improve ECC mechanical properties and material greenness." *ACI Mater. J.*, 104(6), 620–628.